Charting the metabolic landscape of the facultative methylotroph *Bacillus methanolicus*

Baudoin Delépine[a], Marina Gil López[b], Marc Carnicer[a*], Cláudia M. Vicente[a], Volker F. Wendisch[b], Stéphanie Heux[a#]

[a] TBI, Université de Toulouse, CNRS, INRA, INSA, Toulouse, France.

[b] Genetics of Prokaryotes, Faculty of Biology & CeBiTec, Bielefeld University, Bielefeld, Germany

Running Head: Metabolic states of the methylotroph *B. methanolicus*

Address correspondence to SH, heux@insa-toulouse.fr

Post: TBI - INSA de Toulouse, 135 avenue de Rangueil, 31077 Toulouse CEDEX 04; Phone number: +33 (0)5 61 55 93 55

* Present address: IQS, Universitat Ramon Llull, Via Augusta 390, E-08017, Barcelona, Spain

ACKNOWLEDGEMENT

MetaToul (www.metatoul.fr), which is part of MetaboHub (ANR-11-INBS-0010, www.metabohub.fr) are gratefully acknowledged for their help in collecting, processing and interpreting 13-C NMR and MS data. We would like to thank Marcus Persicke, Maud Heuillet, Edern Cahoreau, Lindsay Periga, Pierre Millard, Gilles Vieira and Jean-Charles Portais for the insights they provided.

FUNDING

This work was supported by ERA-CoBioTech's project C1Pro (ANR-17-COBI-0003-05 and FNR-22023617).

ABSTRACT

Abstract

Bacillus methanolicus MGA3 is a thermotolerant and relatively fast-growing methylotroph able to secrete large quantities of glutamate and lysine. These natural characteristics make *B. methanolicus* a good candidate to become a new industrial chassis organism, especially in a methanol-based economy. This has motivated a number of omics studies of *B. methanolicus* at the genome, transcript, protein and metabolic levels. Intriguingly, the only substrates known to support *B. methanolicus* growth as sole source of carbon and energy are methanol, mannitol, and to a lesser extent glucose and arabitol. We hypothesized that comparing methylotrophic and non-methylotrophic metabolic states at the flux level would yield new insights into MGA3 metabolism. ^{13}C metabolic flux analysis (^{13}C-MFA) is a powerful computational method to estimate carbon flows from substrate to biomass (i.e. the *in vivo* reaction rates of the central metabolic pathways) from experimental labeling data. In this study, we designed and performed a ^{13}C-MFA of the facultative methylotroph *B. methanolicus* MGA3 growing on methanol, mannitol and arabitol to compare the associated metabolic states. The results obtained validate previous findings on the methylotrophy of *B. methanolicus*, allowed us to characterize the assimilation pathway of one of the studied carbon sources, and provide a better overall understanding of this strain.

Importance

Methanol is cheap, easy to transport and can be produced both from renewable and fossil resources without mobilizing arable lands. As such, it is regarded as a potential carbon source to transition toward a greener industrial chemistry. Metabolic engineering of bacteria and yeast able to efficiently consume methanol is expected to provide cell factories that will transform methanol into higher-value chemicals in the so-called methanol economy. Toward that goal, the study of natural methylotrophs such as *B. methanolicus* is critical to understand the origin of their efficient methylotrophy. This knowledge will then be leveraged to transform such natural strains into new cell factories, or to design methylotrophic capability in other strains already used by the industry.

KEYWORDS

Natural methylotrophy, 13C metabolic flux analysis, non-stationary MFA, Bacillus methanolicus MGA3, methanol

Abbreviations

^{13}C-MFA: ^{13}C metabolic flux analysis; CID: carbon isotopologue distribution; FBA: Flux Balance Analysis; MS: mass spectrometry; NMR: nuclear magnetic resonance; PTS: phosphotransferase system

Pathways

SBPase: fructose bisphosphate aldolase/sedoheptulose bisphosphatase; TA: fructose bisphosphate aldolase/transaldolase; PPP: pentose phosphate pathway; RuMP: Ribulose Monophosphate Cycle; TCA: Krebs cycle

Reactions

akgdh: 2-oxoglutarate dehydrogenase and 2-oxoglutarate synthase; Araupt: arabitol uptake; detox: linear detoxification pathways; fum: fumarate reductase; glpx: sedoheptulose-bisphosphatase; gnd: phosphogluconate dehydrogenase; hps: 3-hexulose-6-phosphate synthase ; idh: isocitrate dehydrogenase; Manupt: mannitol uptake; mdh: methanol dehydrogenase; pdh: pyruvate dehydrogenase; pfk: 6-phosphofructokinase and fructose-bisphosphatase; pgi: glucose 6-phosphate isomerase ; pgk: glyceraldehyde 3-phosphate dehydrogenase, phosphoglycerate kinase, and phosphoglycerate mutase; phi: 6-phospho-3-hexuloisomerase ; pyk: pyruvate kinase; rpe: ribulose-phosphate 3-epimerase; rpi: ribose 5-phosphate isomerase; rpi: ribulose phosphate isomerase; ta: transaldolase; tkt1, tkt2: transketolases; zwf: glucose-6-phosphate dehydrogenase and 6-phosphogluconolactonase.

Metabolites

Ace: acetate; Aco: aconitate; AKG: 2-oxoglutarate; ala: alanine; Ara: arabitol; arg: arginine; asp: aspartate; Cit: citrate; DHAP: dihydroxyacetone phosphate; Ery4P: erythrose 4-phosphate; For: formaldehyde; Fru6P: fructose 6-phosphate; FruBP: fructose 1,6-bisphosphate; Fum: fumarate; G3P: 3-phospho-D-glycerate; GAP: glyceraldehyde 3-phosphate; Glc6P: glucose 6-phosphate; glu: glutamate; gly: glycine; GlyOx: glyoxylate; Gnt6P: 6-phosphogluconate; Hex6P: hexulose 6-phosphate; his: histidine; ile: isoleucine; leu: leucine; lys: lysine; Mal: malate; Man: mannitol; MeOH: methanol; met: methionine; OAA: oxaloacetate; PEP: phosphoenolpyruvate; PGA: 2-phospho-D-glycerate; phe: phenylalanine; pro: proline; Pyr: pyruvate; Rib5P: ribose 5-phosphate; Ribu5P: ribulose 5-phosphate; Sed7P: sedoheptulose 7-phosphate; ser: serine; Suc: succinate; thr: threonine; tyr: tyrosine; val: valine; Xyl5P: xylulose 5-phosphate.

1. INTRODUCTION

^{13}C metabolic flux analysis (^{13}C-MFA) has emerged in the last decade as an outstanding experimental method to describe the metabolic states of microorganisms. It has successfully been used to identify new pathways (1), investigate responses to environmental changes (2), improve the titer of cell factories (3), screen strains based on their enzymatic capacity (4), and more generally to provide a better understanding of the metabolism of microorganisms (5) such as methylotrophs (6–8). Briefly, ^{13}C-MFA exploits a metabolic model and ^{13}C-isotope patterns measured from key metabolites to estimate reaction rates consistent with the observed labeling patterns (see (9, 10) for reviews). Specifically, cells are grown on a ^{13}C labeled carbon source, metabolites of the central metabolism or constituents of the biomass such as proteinogenic amino acids are sampled and quenched, and their carbon isotopologue (i.e. labeling) distribution (CID) is measured by mass spectrometry (MS) and/or nuclear magnetic resonance (NMR). A metabolic model is then used to fit these measurements to theoretical CID data that are simulated by optimizing reaction flux values from the metabolic model. Assuming mass balance, if the measurements are coherent and the topology of the metabolic model is correct, the experimental and simulated data will converge, yielding the estimated reaction fluxes. Finally, ^{13}C-MFA provides a flux map: a predicted snapshot of the metabolic fluxes through the organism of interest during the experiment, i.e. its metabolic state. ^{13}C-MFA flux maps are conceptually similar to those from flux balance analysis (FBA), a purely *in*

silico method that, from a metabolic model (typically at the genome scale), computes the optimal reaction flux distribution to maximize an objective defined in terms of metabolite production, often designed to model cell growth. Importantly, ^{13}C-MFA flux maps are estimates based on experimental data, whereas FBA flux maps are purely *in silico* predictions, which can be confirmed by gene deletion analysis or ^{13}C-MFA for example.

Bacillus methanolicus MGA3 is a gram-positive bacterium that was first isolated in the 1990s from freshwater marsh soil samples after an enrichment culture on methanol at 55 °C (11). Its ability to grow quickly and to secrete large quantities of glutamate and lysine in methanol at high temperature make it a good candidate for biotech applications. Methanol is indeed viewed as a promising renewable feedstock because of its abundance and low price (12, 13), while high temperature cultures are less prone to contamination and require less cooling when scaled up (14). Furthermore, *B. methanolicus* is able to grow in seawater, which is also cheap and abundant (15). Promising metabolic engineering studies have already established MGA3 as a cell factory for the heterologous production of cadaverine (16) and GABA (17). While the lack of genetic tools must have impaired the development of new applications in the past (18), the establishment of gene expression tools based on theta- and rolling-circle replicating plasmids have made *B. methanolicus* amenable to the overproduction of amino acids and their derivatives (19), and there is hope that recent breakthroughs from CRISPR interference (CRISPRi) will stimulate new innovations (20).

As a facultative methylotroph, *B. methanolicus* MGA3 can also grow on non-methylotrophic substrates such as D-mannitol, D-glucose and D-arabitol. The metabolic pathways involved in the uptake of mannitol and glucose have been described (21), as has the organization of genes involved in mannitol utilization (19). Both substrates enter the cells via a phosphotransferase system (PTS), respectively as mannitol 1-phosphate and glucose 6-phosphate, and are further converted to fructose 6-phosphate. Arabitol has recently been characterized as a fourth source of carbon and energy for *B. methanolicus* (22). The operon responsible for arabitol assimilation was identified as harboring a PTS system (AtlABC) and two putative arabitol phosphate dehydrogenases (AtlD and AtlF), whose activities were demonstrated in crude extracts. However, as the pathway was not completely characterized, it is unclear whether arabitol is assimilated through arabitol 1-phosphate to xylulose 5-phosphate (Xyl5P), or to ribulose 5-phosphate (Ribu5P) through arabitol 5-phosphate. It has been suggested that both routes operate in parallel in *Enterococcus avium* and other gram-positive bacteria (23). A series of omics studies comparing these carbon sources with methanol have contributed to a better understanding of *B. methanolicus* metabolism at the genome (21, 24), transcriptome (21, 22, 25), proteome (26) and metabolome levels (27, 28). However, a flux level description, which could validate previous findings and provide new insights into the facultative methylotrophy of *B. methanolicus* and its associated metabolic states, is still lacking.

In this study, we designed and performed ^{13}C-MFA of the facultative methylotroph *Bacillus methanolicus* MGA3 growing on methanol, mannitol and arabitol. Methanol (CH_4O) and mannitol ($C_6H_{14}O_6$) are the best known carbon sources for this strain (11, 14), with comparable growth rates; while growth on arabitol ($C_5H_{12}O_5$) is significantly slower (22) and its assimilation pathway has not yet been fully described. All three carbon sources are probably present in MGA3's natural habitats, on plant leaves (29) or as plant degradation products (30). With their wide availability and fast associated growth rate, methanol and mannitol are promising feedstocks for industrial applications, while arabitol growth allows the facultative methylotrophy of MGA3 to be studied with a less efficient C source and to finish characterizing its assimilation pathway.

2. MATERIALS & METHODS

2.1 Strain

B. methanolicus wild-type MGA3 (ATCC 53907) strain was used for metabolic flux analyses. Strains used for cloning and expression are described in the section 2.5.1 and listed in Table 1.

2.2 Non-stationary ^{13}C fluxomics experiment

2.2.1 Culture conditions and parameters

For the carbon source methanol, two batch cultures were performed in 0.5 litre bioreactors (INFORS HT Multifors, The Netherlands) with a working volume of 0.40 litres coupled to a Dycor ProLine Process Mass Spectrometer (AMETEK Process Instruments, USA). The culture medium per litre was: 3.48 g $Na_2HPO_4 \cdot 12\ H_20$, 0.606 g KH_2PO_4, 2.5 g NH_4Cl, 0.048 g yeast extract, 1 ml of 1 M $MgSO_4$ solution, 1 ml of trace salt solution, 1 ml of vitamins solution, 0.05 ml Antifoam 204 and 150 mM of methanol. The trace salt solution per litre was: 5.56 g $FeSO_4 \cdot 7\ H_2O$, 0.027 g $CuCl_2 \cdot 2\ H_2O$, 7.35 $CaCl_2 \cdot 2\ H_2O$, 0.040 g $CoCl_2 \cdot 6\ H_2O$, 9.90 g $MnCl_2 \cdot 4\ H_2O$, 0.288 g $ZnSO_4 \cdot 7\ H_2O$ and 0.031 g H_3BO_3. The vitamin solution per litre was: 0.10 g D-biotin, 0.10 g thiamine·HCl, 0.10 g riboflavin, 0.10 g pyridoxine·HCl, 0.10 g pantothenate, 0.10 g nicotinamide, 0.02 g p-aminobenzoic acid, 0.01 g folic acid, 0.01 g vitamin B12 and 0.01 g lipoic acid. The pre-cultures were grown in two half

litre shake flasks containing 150 ml of the pre-culture medium and inoculated with cryostock of *B. methanolicus* wild-type MGA3 cells. The cultures were grown overnight at 50 °C under shaking at 200 rpm, and used to inoculate the reactors. The aeration rate of 1 vvm was controlled by a mass flow meter (INFORS HT Multifors, The Netherlands) and pO2 were maintained above 25 % throughout all cultures. Temperature, pH and stirring speed were maintained at 50 °C, pH 6.8 (with KOH 1 M) and 800 rpm, respectively. The N_2, O_2, Argon, CO_2, ^{13}C-CO_2 and methanol concentrations in the bioreactors off-gas were measured on-line with the mass spectrometer.

To perform the pulse of tracer, 100 mM of ^{13}C-methanol (99 % ^{13}C; Euriso-Top, France) were added to the cultures at an OD_{600} of 2.5. Growth curves are available in Supplementary Data 1.

2.2.2 Quantification of cells and supernatant NMR analysis

For determination of the dry weight of cells, a conversion factor of 0.389 g/l (dry weight) of cells per OD_{600} unit was used. Supernatant samples were taken to analyse substrate methanol consumption as well as by-product formation by subtracting 1 ml of culture and centrifuged it at 13000 × *g* for 60 s. Thereafter, supernatant was collected and stored until analysis at -20 °C. Supernatant analysis was performed by ^{1}H 1D-NMR at 292 °K, using a 30° pulse and a relaxation delay of 20 s, with an Avance 800 MHz spectrometer (Bruker, Germany). Deuterated trimethylsilyl propionate (TSP-d4) was used as an internal standard for quantification.

2.2.3 Sampling and MS analysis of intra and extracellular pool sizes

When the cultures reached an OD_{600} of 2, metabolome samples were collected using the optimized method described by (28). Briefly, total broth quenching with correction for metabolites in the extracellular medium was performed in quadruplicates to assess the metabolite pool sizes in the two cultivations performed. Metabolites pool sizes were quantified (Fig. S1) by ion chromatography tandem mass spectrometry (IC-MS/MS) using cell extract of *Escherichia coli*, cultivated on 99 % [$^{13}C_6$] glucose (Euroisotop, France), as internal standard (31). Liquid anion exchange chromatography was performed as described previously (32).

2.2.4 Sampling and MS analysis of labeled metabolites

Label enrichments in the intracellular metabolites were followed after performing a pulse of 100 mM ^{13}C-methanol at an OD_{600} 2.5. Whole broth (internal + external pools; WB) and culture filtrate (external pools; CF) were sampled to indirectly track label incorporation in the intracellular metabolites. Specifically, 13 WB and 3 CF samples were collected in 3.5 min in each bioreactor. Exact sampling times can be seen in Supplementary Data 1. IC-MS/MS quantification was used to analyse the isotopologues of each metabolite as described by (32). The metabolites analysed were PEP, Rib5P+Ribu5P+Xyl5P, Sed7P, Gnt6P, Glc6P, FruBP, Fru6P, Gly3P, 13PG, G3P+PGA, Cit, Aco, Fum, Mal and Suc. After manual peak integration, the raw peak areas were corrected for the contribution of all naturally abundant

isotopes using IsoCor software (33). Some cross-contamination was found in the isotopologues M4 of Aco and M2 and M3 of Gnt6P that were subsequently removed from the analysis (Supplementary Data 1).

Additionally, the exact ratio between ^{13}C-methanol and ^{12}C-methanol after the pulse was measured by ^{1}H 1D-NMR as well as the evolution of $^{12}CO_2$ and $^{13}CO_2$ by the mass gas analyser.

2.2.5 Mass balance

Experimental data consistency of the measured rates was verified using standard data reconciliation procedures under the elemental mass balance constraints (34). The biomass elemental composition used in the reconciliation procedure was taken from the closely related non-methylotrophic bacterium *Bacillus subtilis*, $CH_{1.646}N_{0.219}O_{0.410}S_{0.005}$ (35, 36). The ashes content were considered to be 6 % of the dry cell weight, average value obtained from different microorganisms (i.e. *Escherichia coli, Aspergillus niger, Penicicillium chrysogenum, Klebsiella aerogenes* (37)). After no proof of mismatch in the measurements, a better estimation of the physiological parameters were obtained as described by (34).

2.3 Stationary ^{13}C fluxomics experiments

2.3.1 Culture conditions

For the carbon sources mannitol and arabitol, the culture medium composition remained unchanged. The experiments were performed in

500 ml baffled shake flasks using 40 ml of media, and cells were grown at 50 °C and 200 rpm. Pre-cultures contained yeast extract and 15 mM unlabeled mannitol or arabitol. They were inoculated as stated previously and grown overnight. The pre-cultures were used to inoculate triplicate main cultures to an OD_{600} of 0.05, after centrifugation and re-suspension in media without yeast extract. The media to perform the ^{13}C MFA contained 15 mM [1-^{13}C] mannitol, 15 mM [5-^{13}C] arabitol or 15 mM of a mixture of 10 % [1-^{13}C] arabitol and 90 % [2-^{13}C] arabitol (99 % ^{13}C; Omicron Biochemicals, Inc., South Bend, IN, USA). An experimentally determined conversion factor of 0.22 g/litre (dry weight) of cells per OD_{600} unit was used. Growth curves are available in Supplementary Data 1.

2.3.2 Measurements of proteinogenic amino acids ^{13}C-isotopologues

Mannitol (resp. arabitol) cultures were sampled around 10 h (resp. 30 h) once they reached an OD_{600} of 1.3. The pellets obtained from the cellular extract were hydrolyzed 15 h at 110 °C with 500 µl HCL 6N. Samples were evaporated and washed twice with 500 µl of ultrapure water, evaporated to dryness, resuspended (625 µl, water), and diluted (1/1000, water) for the mass spectrometry analysis.

Amino acids were separated on a PFP column (150 × 2.1 mm i.d., particle size 5 µm; Supelco Bellefonte, PEN, USA). Solvent A was 0.1 % formic acid in H_20 and solvent B was 0.1 % formic acid in acetonitrile at a flow rate of 250 µL/min. The gradient was adapted from the method used by (38).

Solvent B was varied as follows: 0 min, 2 %; 2 min, 2 %; 10 min, 5 %; 16 min, 35 %; 20 min, 100 %; and 24 min, 100 %. The column was then equilibrated for 6 min at the initial conditions before the next sample was analyzed. The volume of injection was 20 µL.

High-resolution experiments were performed with an Ultimate 3000 HPLC system (Dionex, CA, USA) coupled to an LTQ Orbitrap Velos mass spectrometer (Thermo Fisher Scientific, Waltham, MA, USA) equipped with a heated electrospray ionization probe. MS analyses were performed in positive FTMS mode at a resolution of 60 000 (at 400 m/z) in full-scan mode, with the following source parameters: the capillary temperature was 275 °C, the source heater temperature, 250 °C, the sheath gas flow rate, 45 a.u. (arbitrary unit), the auxiliary gas flow rate, 20 a.u., the S-Lens RF level, 40 %, and the source voltage, 5 kV. Isotopic clusters were determined by extracting the exact mass of all isotopologues, with a tolerance of 5 ppm. Experimental CIDs of alanine, glycine, valine, serine, threonine, phenylalanine, aspartate, glutamate, histidine, isoleucine, leucine, lysine, arginine, tyrosine, proline and methionine were obtained after correction of raw MS data for naturally occurring isotopes other than carbon, using IsoCor (33).

Careful inspection of the CID revealed an overall excellent reproducibility between both the technical and biological replicates (Supplementary Data 1). However, M0 of valine and M0-M1 of glycine had a higher variability which could be due to a signal closer to the noise level.

2.3.3 NMR measurements

Concentrations in supernatants were measured by ^{1}H 1D-NMR at 290 °K, using a 30° angle pulse and a presaturation of water signal was applied during a relaxation delay of 8 s. TSP-d4 was used as internal standard for calibration and quantification.

The measurement of isotopomers and specific enrichments of targeted biomass components were performed using the same samples used for proteinogenic amino acids ^{13}C-isotopologues MS analysis, redried and suspended in 200 µl D_2O (0.1 % DCl). The positional isotopomer distribution of alanine C2 and C3 was extracted from the analysis of ^{13}C–^{13}C couplings in 2D ^{1}H–^{13}C HSQC experiments (39). The carbon isotopic enrichments of alanine (C2 and C3) and histidine (C2 and C5) were extracted from the analysis of ^{1}H–^{13}C couplings using 2D-zero quantum filtered-TOCSY (ZQF-TOCSY) (40).

NMR spectra were collected on an Avance III 800 MHz spectrometer (Bruker, Germany), equipped with a 5mm z-gradient QPCI cryoprobe. Every acquisition 1D, 2D and absolute quantification were performed on ^{1}H-1D spectra using TopSpin 3.5 (Bruker, Germany).

2.4 Models and simulations

2.4.1 Metabolic Flux Analysis software

All simulations needed for Metabolic Flux Analysis (MFA) on methanol, mannitol and arabitol were performed with *influx_si* software v4.4.4 (41), either in stationary or non-stationary mode. *influx* has the advantage to allow for the integration of labeling data coming from different experimental setups (MS, NMR) and to support several integration strategies (stationary, non-stationary, parallel labeling).

All input and output files needed for reproducibility are available in an archive in Supplementary Data 2. Importantly, this includes the models in FTBL and SBML file formats.

2.4.2 Metabolic models

We designed the models to cover central carbon metabolism and biomass needs of *B. methanolicus*. *influx_si* uses a non-standard legacy file format (FTBL) to encode the metabolic network and the associated atom-atom transitions. This format centralizes the metabolic network with all biological measurements, i.e. metabolites pool sizes, fluxes, and carbon isotopologue distribution. Consequently, we developed distinct model files for each carbon source. Models share the same nomenclature and the same general topology between them, which is displayed in Fig. 1 and detailed in Supplementary Data 1.

Assimilation pathways of methanol, mannitol and arabitol were included when relevant to explain the incorporation of the tracer. The CO_2 pool was explicitly modeled within the system to allow for re-incorporation of tracer via CO_2. Amino acids synthesis pathways were modeled as part of biomass needs along with important precursors. Biomass equation was borrowed from *Bacillus subtilis* genome-scale model (42). Reaction for phosphoenolpyruvate carboxykinase (BMMGA3_RS13120) was not included in the final model as the associated expression level was rather low in proteomics (26) and transcriptomics studies (21, 25).

Unless otherwise stated, each culture replicate was processed independently to estimate fluxes for their respective carbon source condition.

For MFA on mannitol, we exploited carbon isotopologue distribution data of proteinogenic alanine, glycine, valine, serine, threonine, phenylalanine, aspartate, glutamate, histidine, isoleucine, leucine, lysine, arginine, tyrosine, proline and methionine. Acetate production was modeled with an export flux from acetyl-CoA to which we associated the acetate flux measured from supernatant data. Acetyl-CoA was further constrained using acetate positional labeling measured by ^{1}H 1D-NMR spectroscopy from the supernatant.

For MFA on arabitol, we averaged the proteinogenic labeling measurements of the [5-^{13}C] arabitol experiment and exploited it as a parallel labeling dataset for each biological replicate of the [1/2-^{13}C] arabitol experiment. We analysed the same proteinogenic amino acids as those mentioned above for

mannitol. No acetate was observed in the supernatant and the associated export reaction was consequently excluded from this model. Additionally, we exploited specific labeling enrichment of histidine, alanine and ribulose-5-P, and positional isotopomer data of alanine from labeling samples as described in section 2.3.3.

For MFA on methanol, the non-stationary nature of the experiment and the subsequent importance of the pools on flux distributions forced us to explicit most of the reactions of the central metabolism that were lumped for the stationary models. Measurements described above were used to constrain intra and extracellular pools (section 2.2.3), and isotopologues profiles (section 2.2.4) through *influx_si* optimization process. The exchange fluxes of CO_2 and methanol (feed and evaporation) were also exploited. No acetate production was observed.

2.4.3. Quality checks

Experimental data were fitted to our models as per described above. For each culture replicate we performed a Monte Carlo sensitivity analysis (n=100) on the fit to assess its robustness to small variations around the fitted values. We also performed a chi-squared goodness-of-fit statistical test to ensure that simulated data for each biological replicate were significantly close to experimental data. All tests were significant with a significance level (α) of 0.05 (Supplementary Data 2). For convenience, we provide figures of measured vs. simulated data points (Fig. S3).

Let us note here that we unfortunately were unable to estimate at a satisfactory precision the fluxes through malate dehydrogenase (BMMGA3_RS12590, 1.1.1.37), malic enzyme (*mae*, BMMGA3_RS12650, 1.1.1.38 or 1.1.1.40) and pyruvate carboxylase (*pyc*, BMMGA3_RS05255, 6.4.1.1). Those three reactions formed a cycle from pyruvate (Pyr) to oxaloacetate (OAA) and malate (Mal) in all our tested models. However, the Monte Carlo sensitivity analysis revealed that those fluxes were statistically undefined (not shown), meaning that virtually any value through the cycle would satisfy the constraints of the rest of the network. In the absence of biological data to motivate any new constraint on the model, we preferred to leave those reactions out of the analysis.

2.5 Analysis of arabitol phosphate dehydrogenases AtlD and AtlF

2.5.1 Strains and culture conditions

In this study, *Escherichia coli* DH5α (43) was used as the standard cloning host and recombinant protein production was carried out with *E. coli* BL21(DE3) (44). A summary of the strains, primers and plasmids constructed and used in this study can be found in Table 1. *E. coli* strains were routinely cultivated at 37 °C and 180 rpm in Lysogeny Broth (LB) medium or on LB agar plates supplemented with 100 µg ml^{-1} ampicillin and 0.5 mM IPTG when relevant.

2.5.1 Recombinant DNA work

Molecular cloning was performed as previously described (45) using primer sequences listed in Table 1. Total DNA isolation from *B. methanolicus* was performed as described in (46). Inserts were amplified by polymerase chain reactions (PCRs) with ALLin™ HiFi DNA Polymerase (HighQu, Kraichtal, Germany) and purified with the NucleoSpin® Gel and PCR Clean-up kit (Macherey-Nagel, Düren, Germany). Plasmids were constructed from PCR-generated fragments and pET16b vector cut with restriction enzymes using the isothermal DNA assembly method (47). The GeneJET Plasmid Miniprep Kit (Thermo Fisher Scientific, Waltham, USA) was used for plasmid isolation. For the transformation of chemically competent *E. coli* cells, the procedure described by (48) was followed. Colony PCRs were performed using Taq polymerase (New England Biolabs, Ipswich, England) with primers P192, P193, P194 and P195 (Table 1). All cloned DNA fragments were verified by sequencing (Sequencing Core Facility, Bielefeld University).

2.3.2 Overproduction and purification of AtlD and AtlF

Plasmids for protein production using *E. coli* BL21 (DE3) were constructed on the basis of pET16b (Novagen, Madison, WI, USA) and are presented in Table 1. The *atlD* and *atlF* genes were PCR-amplified from *B. methanolicus* MGA3 genomic DNA using the primers P192 and P193 or P194 and P195, respectively (Table 1). The resulting product was joined with *Bam*HI digested pET16b by applying the isothermal DNA assembly method (47), resulting in pET16b-*atlD* and pET16b-*atlF*. The pET16 vector allows for production of N-

446 terminal His_{10}-tagged proteins. Protein production and purification was
447 performed following the indications of (49), except for cell lysis which was
448 performed by sonication (UP 200 S, Dr. Hielscher GmbH, Teltow, Germany) on
449 ice at an amplitude of 55 % and a duty cycle of 0.5 for 8 min with a pause in
450 between. Supernatants were subsequently filtered using a 0.2 µm filter and
451 purified by nickel affinity chromatography with nickel-activated nitrilotriacetic
452 acid-agarose (Ni-NTA) (Novagen, San Diego, CA, USA). His-tagged AltD and
453 AtlF proteins eluted with 20 mM Tris, 300 mM NaCl, 5 % (vol/vol) glycerol and
454 50, 100, 200, or 400 mM imidazole were analysed by 12 % SDS-PAGE (50).
455 Fractions showing the highest protein concentrations (with 100 and 200 mM
456 or 100, 200 and 400 mM imidazole for AtlD and AtlF, respectively) were
457 pooled and protein concentration was measured according to the Bradford
458 method (51) using bovine serum albumin as reference. The purified protein
459 was subsequently applied for enzymatic assays.

460 2.3.3 Arabitol phosphate dehydrogenase enzymatic assays

461 Determination of purified AtlD and AtlF activities in the reductive reaction
462 using Xyl5P or Ribu5P as substrate were performed as previously described
463 (23). The assay mixture contained 20 mM Tris-HCl buffer (pH 7.2), 1 mM DTT,
464 0.04 to 0.3 mM NADH or NADPH, 0.03 to 0.6 mM Xyl5P or 0.2 to 4 mM Ribu5P
465 and 0.01 to 0.04 mg AtlD or 0.2 to 0.4 mg AtlF in a total volume of 1 ml. The
466 oxidation rate of NADH or NADPH was monitored at 340 nm and 30 °C for 3
467 min using a Shimadzu UV-1202 spectrophotometer (Shimadzu, Duisburg,
468 Germany). In order to confirm the presence of arabitol phosphate in the
469 enzyme reactions after reduction of Xyl5P and Ribu5P, samples were

subjected to liquid chromatography-mass spectrometry (LC-MS) analyses following the procedure described in (52).

2.4 Data availability

Gene locii mentioned throughout the text are from NCBI annotation of *B. methanolicus* MGA3 genome NZ_CP007739.1 (https://www.ncbi.nlm.nih.gov/nuccore/NZ_CP007739.1).

Supplementary Data 1 contains growth curves, processed MS and NMR data and a summary of the reactions modeled.

Supplementary Data 2 contains raw models, input and output files for influx software and can be downloaded from https://fairdomhub.org/data_files/3269?version=1.

3. RESULTS & DISCUSSION

3.1 *In vitro* assessment of arabitol assimilation

The operon responsible for arabitol assimilation in *B. methanolicus* consists of a PTS system (AtlABC) and two putative arabitol phosphate dehydrogenases (AtlD and AtlF) (22), which are chromosomally encoded and belong to the diverse superfamily of medium-chain dehydrogenases/reductases (MDRs). However, the physiological roles of AtlD and AtlF have not been described to date. Members of the MDR superfamily have high sequence conservation, but sequence-based prediction of their substrate scope is difficult since wide substrate specificity is common (53, 54) (see Supplementary Text for a discussion of their phylogeny). The substrate selectivity of AtlD and AtlF was therefore studied to identify whether arabitol is assimilated via arabitol 1-phosphate dehydrogenase to Xyl5P, and/or to Ribu5P via arabitol 5-phosphate dehydrogenase (23) (Fig. 2). The enzymes were purified as N-terminally His-tagged proteins from recombinant *E. coli* by nickel chelate chromatography. Arabitol phosphate oxidation could not be assayed because there are no commercial arabitol 1-phosphate or arabitol 5-phosphate standards. Therefore, the reverse reaction was tested, as described in material and methods section 2.3.3, with either Xyl5P or Ribu5P as substrate for NAD(P)H dependent reduction. A number of potential sugars (D-ribose, D-fructose, D-xylose, D-mannose, L-arabinose, D-arabinose, L-sorbose, D-galactose, D-glucose, ribose 5-phosphate, glucose 6-

phosphate, glucose 1-phosphate, fructose 6-phosphate and fructose 1-phosphate) and sugar alcohols (D-arabitol, D-mannitol, D-galactitol, D-sorbitol, L-arabitol, D-maltitol, D-xylitol, ribitol and meso-Erythritol) were also tested as substrates but no significant activity (i.e. > 0.05 U mg^{-1}) was detected. The kinetic parameters measured for AtlD and AtlF reduction using either Xyl5P or Ribu5P as substrate are summarized in Table 2. The K_M of 0.07 ± 0.03 mM for AtlD with Xyl5P as substrate and NADH as cofactor was 2.5 times lower than the value obtained for AtlF (0.18 ± 0.05 mM). With Ribu5P as substrate, the K_M for AtlD was 17 times lower (1.21 ± 0.42 mM) (Table 2), and for AtlF, no activity was detected. The V_{max} for AtlD with Xyl5P as substrate and NADH as cofactor was 2.7 times higher than with Ribu5P as substrate (0.49 ± 0.06 U mg^{-1}) and 12 times higher than for AtlF with Xyl5P (0.11 ± 0.01 U mg^{-1}) (Table 2). NADH was the preferred cofactor over NADPH with a ten times lower K_M (0.01 ± 0.01 vs 0.11 ± 0.09 mM). The affinity and NADPH dependent activity (0.24 ± 0.06 U mg^{-1}) could only be determined with AtlD and Xyl5P, as no significant activity was detected for any of the other reactions. LC-MS analyses were performed to confirm the formation of arabitol phosphate in the enzyme reactions catalyzed by AtlD. Although arabitol 1-phosphate and arabitol 5-phosphate could not be distinguished, arabitol phosphate was clearly produced with both Xyl5P and Ribu5P as substrates (Fig. S2).

Overall, these data suggest that AtlD has a major role in arabitol catabolism *in vitro* and that AtlD and AltF both prefer Xyl5P. This suggests that arabitol is mainly assimilated through the arabitol 1-phosphate pathway. However,

assimilation via arabitol 5-phosphate cannot be excluded since AtlD can also use Ribu5P, albeit with reduced efficiency as shown both by the kinetic parameters (Table 2) and the significant residual Ribu5P detected in the enzyme reactions (Fig. S2). Moreover, *in vitro* enzymatic analyses of purified arabitol phosphate dehydrogenase from *E. avium* (23) and *Bacillus halodurans* (55) showed that both could convert arabitol 1-phosphate and arabitol 5-phosphate into both Xyl5P and Ribu5P. By assessing metabolic operations *in vivo*, ^{13}C-MFA experiments should identify which assimilation pathway is actually used *in vivo*.

3.2 ^{13}C-MFA experimental design

Experimental design is a key step to define the isotopic composition of the label input and the isotopic data to be measured, thereby improving both the number of fluxes that can be estimated from a set of isotopic data and the precision of the flux values. To address this point, we used a dedicated program, IsoDesign (56), using as input metabolic models of each carbon source and several labels as described in the material and methods section. For arabitol and mannitol, good flux precision could be obtained with mass spectrometry labelling data from proteinogenic amino acids. This is advantageous for two reasons. First, the experimental setup is simpler than for intracellular metabolites because no quenching is required and the cellular pellet can just be collected by centrifugation. Second, the labelling can be measured by NMR and MS, providing crucial positional information to distinguish between the two pathways (i.e. via arabitol 5-phosphate or via

arabitol 1-phosphate dehydrogenase). Among the different label inputs tested, 100% [5-^{13}C] arabitol appeared ideal to identify whether arabitol is converted into arabitol 1-phosphate only or into arabitol 5-phosphate only. In addition, a 9:1 mix of [1-^{13}C] and [2-^{13}C] arabitol was used to see if both pathways are active. For mannitol, the best label input was 100 % [1-^{13}C]. Finally, since methanol is a C1 compound, a stationary ^{13}C-MFA approach is not suitable since the amino acids become fully labeled in the isotopic steady-state. Non-stationary ^{13}C fluxomics should be used instead to follow the incorporation of the tracer after a pulse of labeled substrate; however significantly more ^{13}C data are required for this approach (57, 58) (Supplementary Data 1).

All labeling samples were collected in the exponential growth phase at metabolic steady state and analyzed by MS or 1D ^{1}H NMR. The labelling profile of the analyzed metabolites, as measured by their CIDs, were inspected manually and then used with additional NMR and physiological data to fit a model of *B. methanolicus*'s central metabolism (Supplementary Data 1).

3.3. Measurement of physiological parameters

Assessment of physiological parameters is a prerequisite for flux calculation. Here, *B. methanolicus* was grown in batch on three different carbon sources. For each cultivation, growth rate and consumption and production rates were determined. Results are given in Table 3. No significant differences between the physiological parameters obtained for the culture replicates were

observed. On methanol (batch cultures at 50 °C), around 35 % of the carbon source was directly evaporated, and biomass and carbon dioxide were the only products formed in detectable amounts. The maximal growth rate obtained here with methanol (0.46 h^{-1}) is slightly higher than reported in a previous proteomic study of *B. methanolicus* MGA3 (0.40 h^{-1}, (14)) or for the growth of the related strain *B. methanolicus* PB1 (0.32 h^{-1}, (15)). Biomass yields did not differ significantly from 0.5 g/g indicating that approximately half of the consumed methanol went to biomass and the other half was oxidized to CO_2. The growth rates with mannitol and arabitol are consistent with published values (22).

B. methanolicus MGA3 is known to overproduce glutamate at up to 50 g/l (21) on methanol under magnesium or methanol limitation (59, 60). When grown on arabitol or methanol, no metabolite accumulated in the supernatant at concentrations above the NMR detection limit (approximately 100 µM). There was therefore little or no metabolite secretion by MGA3 under our chosen methanol and arabitol growth conditions, which is consistent with previous studies and the growth conditions studied here (27, 28). However, acetate was produced at up to 2 mmol/gDCW/h in mannitol cultures (yield, 0.3 mol/mol). To the best of our knowledge, acetate production has never previously been reported for *B. methanolicus*. Based on genomics data (21), we hypothesized that acetate is synthesized from acetyl-CoA in a classical two-step process involving phosphate acetyltransferase (EC:2.3.1.8, BMMGA3_RS15725) and acetate kinase (EC:2.7.2.1, BMMGA3_RS12735). Acetate has moreover been discussed at length in the context of overflow

metabolism, a special metabolic state in which fermentation pathways are used even though further oxidation (respiration) would be more ATP-efficient (61–64). Overflow metabolism has industrial implications since it could lead to carbon and energy waste.

Overall, we showed the reproducible growth characteristics of our cultures, and showed an unexpected production of acetate that may have an impact for industrial applications, as overflow metabolism leads to carbon and energy waste.

3.4 *In vivo* characterization of arabitol assimilation

The *in vitro* enzymatic analyses of the two dehydrogenases, AltD and AltF, suggest that both assimilation pathways (i.e. via arabitol 1-phosphate and via arabitol 5-phosphate) may operate *in vivo*. To confirm whether either or both arabitol assimilation pathways are operative in *B. methanolicus*, as suggested for *E. avium* (23) and *Bacillus halodurans* (55), we carried out a ^{13}C-MFA specifically designed to discriminate between the two pathways (see section 3.1, and Fig 2). Interestingly, while the possibility to assimilate arabitol through Xyl5P or Ribu5P or both was a free parameter, the optimal solution found during the fitting process exclusively used the route through Xyl5P (Fig. 1C). This indicates that the (low) activity observed *in vitro* through Ribu5P was not present at a detectable level in our cultures, and that the PTS system imports arabitol as arabitol 1-phosphate. The kinetic parameters obtained for AtlD and AtlF are in line with the flux data, i.e. entry of arabitol into the pentose phosphate pathway (PPP) via PTS-mediated uptake and

620 phosphorylation to arabitol 1-phosphate followed by oxidation to Xyl5P with
621 AtlD as the major dehydrogenase (Fig. 2 and Table 2).

622 Overall, these data demonstrate for the first time how arabitol is assimilated
623 in *B. methanolicus* and rule out the hypothesis of additional catabolism
624 through arabitol 5-phosphate and Ribu5P derived from our enzymatic
625 analyses (Table 2) and previous reports in *E. avium* (23) and *B. halodurans*
626 (55).

627 3.5. *In vivo* operation of the pentose phosphate
628 pathway with the different carbon sources

629 *B. methanolicus* assimilates methanol through the ribulose monophosphate
630 (RuMP) cycle that condenses formaldehyde (For) and ribulose 5-P (Ribu5P)
631 into hexulose 6-P (Hex6P) (65). The regenerative part of the RuMP cycle that
632 maintains a pool of Ribu5P overlaps with the non-oxidative pentose
633 phosphate pathway (PPP). Strong flux through the PPP is therefore expected
634 on methanol and indeed, ribulose-phosphate 3-epimerase's relative flux
635 accounted for 67 % of methanol assimilation (*rpe*, Fig. 1A). Interestingly,
636 mannitol and arabitol are closely connected to the PPP since mannitol is
637 converted to fructose 6-P (F6P) (just like methanol), whereas arabitol is
638 converted to Xyl5P as discussed above. On mannitol (Fig. 1B), PPP utilization
639 was low (the estimated *rpe* flux was 15 % of mannitol assimilation), which
640 contrasts with the predominance of the PPP on methanol. On arabitol
641 (Fig. 1C), the fluxes associated with the PPP remained low (*rpe* flux,
642 1.2 mmol/gDCW/h; Fig. 3), but they accounted for a larger fraction of the

643 assimilated carbon flow (the estimated *rpe* flux was 28 % of arabitol
644 assimilation) than on mannitol. This indicates that the PPP is more important
645 for carbon assimilation on arabitol than on mannitol, in spite of similar
646 absolute reaction rates and expression levels (22). Simulations carried
647 without transaldolase activity indicated that it was essential to explain the
648 labeling data given the network topology used (notably *glpx* been
649 irreversible). A possibility for future studies would be to take advantage of
650 adaptive laboratory driven evolution, or overexpression of key enzymes such
651 as transaldolase, to investigate if the PPP could be adjusted to increase
652 growth rates when arabitol is the sole source of carbon and energy.

653 The RuMP cycle has several variants, which differ in their efficiency (66).
654 Genes for two of these have been identified in MGA3, namely, the fructose
655 bisphosphate aldolase/sedoheptulose bisphosphatase (SBPase) cycle (67)
656 and the fructose bisphosphate aldolase/transaldolase (TA) cycle, which as
657 their names suggest favor the regeneration of Ribu5P through sedoheptulose
658 bisphosphatase and transaldolase, respectively. It is generally accepted that
659 MGA3 uses the SBPase variant (65). The main evidence for this is the
660 presence of a copy of a characteristic gene of the SBPase variant ($glpX^{P}$) on
661 the pBM19 plasmid, whereas there is only one transaldolase gene (ta^{C}) in the
662 chromosome. Proteomic (26) and transcriptomic (21) studies have also
663 associated $glpX^{P}$ with a significant increase in expression in methanol
664 compared with mannitol, whereas the expression associated with ta^{C}
665 remained constant. According to the MFA, both *glpx* (associated to $glpX^{P}$) and
666 *ta* (associated to ta^{C}) carry a comparable flux, thus both variant may be

667 active (Fig. 3). This arrangement may serve as a fail-safe to guarantee the
668 replenishment of Ribu5P. Alternatively, since transaldolase activity is
669 essential to fit the isotopic data for growth on arabitol, an advantage of the
670 TA cycle may be that it increases the flexibility of the PPP and allows the
671 regeneration of important precursors such as Ribu5P from different carbon
672 sources.

673 The labeling data suggest that the oxidative part of the PPP is almost shut
674 down on methanol, with an estimated absolute flux of 0.16 mmol/gDCW/h
675 through glucose 6-phosphate isomerase (*pgi*, < 1 % of the flux relative to
676 methanol assimilation, Fig. 3). On mannitol and on arabitol, utilization of the
677 oxidative part of the PPP is higher, with estimated absolute fluxes of 1.87
678 mmol/gDCW/h and 0.53 mmol/gDCW/h, respectively (Fig. 3). This is in
679 contrast with previous findings that suggested that the oxidative part of the
680 PPP might be used on methanol to provide NADPH while detoxifying
681 formaldehyde (14, 27) via the so-called cyclic dissimilatory RuMP pathway
682 (21, 68). This claim is supported by (27), based on the comparable pool sizes
683 and isotopic labeling incorporation rates between metabolites of the PPP and
684 6-phosphogluconate (Gnt6P), a key metabolite of the oxidative part of the
685 PPP. Additionally, glucose 6-phosphate dehydrogenase (*zwf*,
686 BMMGA3_RS06660) has been found to be highly over-expressed in both
687 transcriptomics and proteomics studies on methanol compared to mannitol
688 (14). Nonetheless, the same studies report that the other steps of the
689 oxidative PPP are not over-expressed, which include the decarboxylation
690 conducted by phosphogluconate dehydrogenase (*gnd*, BMMGA3_RS10800).

691 The utilization of the oxidative part of the PPP is of particular interest
692 because, intuitively, one imagines that decarboxylation should be avoided
693 when growth occurs on a C1 to avoid wasting carbon. This intuition proved to
694 be correct in Bennett et al.'s (69) study of an *E. coli* synthetic methylotroph
695 in which they knocked-out *pgi* to increase the regeneration of Ribu5P through
696 the non-oxidative part of the PPP. However, we cannot exclude the possibility
697 that the oxidative part of the PPP serves as a backup formaldehyde
698 dissimilation pathway when the linear dissimilation pathways become
699 saturated at high methanol concentrations. *B. methanolicus* is indeed quite
700 sensitive to variations in methanol concentration (70) and we can assume
701 that this critical biological function is tightly controlled. The true importance
702 of the cyclic dissimilatory RuMP pathway for natural methylotrophic growth is
703 therefore difficult to ascertain without additional experiments to specifically
704 measure utilization of the oxidative part of the PPP at different methanol
705 concentrations.
706 As expected, the ^{13}C-MFA shows that the PPP is critical on methanol as it
707 overlaps with the RuMP responsible for methanol assimilation. The SBPase
708 variant of the RuMP is active, however we could not rule out a parallel
709 operation of the TA variant. We suggest that a parallel operation on mixed
710 carbon sources may benefit *B. methanolicus* to replenish important
711 precursors pools. Surprisingly, the oxidative part of the PPP was inactive in
712 our conditions, which question the true importance of the cyclic dissimilatory
713 RuMP for methylotrophic growth.

3.6 *In vivo* operation of the TCA cycle with the different carbon sources

B. methanolicus has a full gene set for a functional tricarboxylic acid cycle (TCA) and glyoxylate shunt (14, 21). This seems to contrast with some methylotrophs, including some that use the RuMP pathway, that do not need a complete TCA to fulfill their energy requirements (71). Results (Fig. 1A) indicate that the TCA is used much less than the RuMP pathway on methanol, with a rate close to 1 mmol/gDCW/h up to 2-oxoglutarate (AKG) and no flux afterwards (Fig. 3). This small flux is needed to support the synthesis of biomass precursors. On mannitol and arabitol in contrast, the TCA is used intensively, with rates of 3.5 and 4.7 mmol/gDCW/h respectively for isocitrate dehydrogenase (*idh*). These results are in agreement with previous measurements of the actual usage of the TCA during methylotrophic growth. At the transcript and protein levels, it has been suggested that the TCA should be more active on mannitol than on methanol (21, 26). Activity assays in crude cell extracts also showed very low 2-oxoglutarate dehydrogenase (*akgdh*) activity (59). Finally, isotopic labeling experiments have shown slow isotopic enrichment of key TCA metabolites (citrate, 2-oxoglutarate, fumarate) on methanol (27).

Although *B. methanolicus* also has glyoxylate shunt genes (BMMGA3_RS01750, 2.3.3.9; and BMMGA3_RS01755, 4.1.3.1), the reported expression levels suggest that this pathway does not carry a high flux under mannitol or under methanol growth conditions (21, 26). In agreement with

these findings, the glyoxylate shunt fluxes estimated in this study were negligible under all the tested conditions (Fig. 3).

Overall, as reported before, the TCA is mainly active in non-methylotrophic conditions and the glyoxylate shunt was inactive in our conditions.

3.7 Analysis of cofactor usage with the various carbon sources

To assess how *B. methanolicus* balances its redox and energy needs, we used the estimated fluxes from the ^{13}C-MFA to infer production and consumption rates of ATP, NADH and NADPH, as displayed in Fig. 4. ^{13}C-MFA is constrained by carbon balance and the distribution of the isotopic tracer, but unlike flux balance analysis it is typically not constrained by cofactor balance. We used the estimated fluxes from the MFA and the expected stoichiometry of the associated reactions to assess the absolute rates of cofactor production and consumption. In the absence of specific measurements, we use the biomass requirements of *B. subtilis* (7, 72). Additionally, since the samples were collected in metabolic pseudo steady-state, the production and consumption rates of each cofactor were assumed to be balanced; this allowed us to identify rates that would have been impossible to estimate otherwise such as the proportion of NAD (and ATP) formed from the respiratory chain (with a P/O=1.5) and other production/consumption rates not accounted for by our other assumptions.

Despite their different growth rates, which influence their cofactor requirements for growth (Table 3), the cells grown on mannitol and arabitol

had a similar absolute usage of NADH, NADPH and ATP (Fig. 4). ATP and NADH came mostly from the same sources. However, the proportion of NADPH generated in the oxidative part of the PPP was three times higher in mannitol growth conditions than in arabitol (3.5 against 1.0 mmol/gDCW/h). This difference was compensated by a higher flux in the TCA for arabitol (4.7 against 3.5 mmol/gDCW/h) in excess of the estimated NADPH requirements for growth and even contributing to the production of ~3.4 mmol/gDCW/h NADPH whose consumption remains unaccounted for. Discrepancies between estimates of the cofactor requirements for biomass formation and those derived from measured isotopic data are typical for this kind of analysis (73, 74), and can be attributed to an underestimation of cofactor requirements, notably for non-essential processes such as cell motility (for ATP). Note, nevertheless, that the estimated biomass requirement for NADPH was not covered under methanol conditions, as 1.5 mmol/gDCW/h is missing from the balance. This may be due to an unaccounted for NADPH-producing process (75), for instance the malic enzyme (*mae*, 1.1.1.40, BMMGA3_RS12650) whose flux could not be estimated with this approach. To the best of our knowledge, there is no evidence of transhydrogenase activity in *B. methanolicus*.

Comparing methylotrophic and non-methylotrophic growth, it is perhaps unsurprising that NADH is produced at a higher rate on methanol (44 mmol/gDCW/h, versus 30 mmol/gDCW/h on mannitol), because of the conversion of methanol into formaldehyde by methanol dehydrogenase (76). This suggests that at the same growth rate, O_2 consumption should be higher

784 on methanol to provide the additional NAD^+ required. Unlike NADH, the
785 NADPH total production is estimated to be roughly the same across our
786 conditions, around 6 mmol/gDCW/h (Fig. 4). As discussed above, the linear
787 formaldehyde detoxification pathways are extensively used in our methanol
788 conditions, while usage of the oxidative part of the PPP (which would be part
789 of the cyclic dissemination pathway) is negligible. In term of cofactors, this
790 mostly affects the sources used for NADPH formation, as the major source on
791 methanol is the detoxification pathway (4.8 mmol/gDCW/h), while the main
792 sources on mannitol are the oxidative part of the PPP (3.6 mmol/gDCW/h)
793 and the TCA (3.5 mmol/gDCW/h). These estimates suggest that linear
794 detoxification pathways play an important role in the generation of NADPH
795 on methanol, in addition to their established protective function against
796 formaldehyde.
797 Non-methylotrophic growth on mannitol and arabitol share the same features
798 despite their associated different growth rates (with the notable exception of
799 the contribution of the oxidative PPP for NADPH production). On methanol,
800 however, we observe more differences in the origin of cofactors production
801 which clearly highlight a different metabolic state. Importantly, the linear
802 detoxification pathways could have a more important role in cofactor
803 regeneration than what was previously envisioned.

804 3.8. Conclusion

805 In summary, this MFA of *B. methanolicus* MGA3 provides three snapshots of
806 its metabolic states for growth on methanol, mannitol or arabitol. Isotopic

data are consistent with prior knowledge of MGA3 methylotrophy, showing greater flux in the RuMP cycle than in the TCA. The ^{13}C-MFA provided new insights related to the utilization of cyclic RuMP versus linear dissimilation pathways, and between the RuMP cycle variants; and finally, the characterization of the arabitol assimilation pathway was completed using enzymatic data. In futur studies, these validated flux maps will be used as references for constraint based modelling to validate genome-scale model predictions. Overall, the information provided in this work and previous omics studies on *B. methanolicus* metabolism can be used to improve design strategies for new strains (i.e. by multi-omics analysis). The experimental path outlined here likely leads to *B. methanolicus* becoming a viable alternative to existing cell factories.

References

1. Peyraud R, Kiefer P, Christen P, Massou S, Portais J-C, Vorholt JA. 2009. Demonstration of the ethylmalonyl-CoA pathway by using 13C metabolomics. PNAS 106:4846–4851.
2. Fendt S-M, Oliveira AP, Christen S, Picotti P, Dechant RC, Sauer U. 2010. Unraveling condition-dependent networks of transcription factors that control metabolic pathway activity in yeast. Molecular Systems Biology 6:432.
3. Becker J, Zelder O, Häfner S, Schröder H, Wittmann C. 2011. From zero to hero—Design-based systems metabolic engineering of Corynebacterium glutamicum for l-lysine production. Metabolic Engineering 13:159–168.
4. Heux S, Poinot J, Massou S, Sokol S, Portais J-C. 2014. A novel platform for automated high-throughput fluxome profiling of metabolic variants. Metab Eng 25:8–19.
5. Klingner A, Bartsch A, Dogs M, Wagner-Döbler I, Jahn D, Simon M, Brinkhoff T, Becker J, Wittmann C. 2015. Large-Scale 13C flux profiling reveals conservation of the Entner-Doudoroff pathway as a glycolytic strategy among marine bacteria that use glucose. Appl Environ Microbiol 81:2408–2422.
6. Van Dien SJ, Strovas T, Lidstrom ME. 2003. Quantification of central metabolic fluxes in the facultative methylotroph methylobacterium extorquens AM1 using 13C-label tracing and mass spectrometry. Biotechnol Bioeng 84:45–55.
7. Peyraud R, Schneider K, Kiefer P, Massou S, Vorholt JA, Portais J-C. 2011. Genome-scale reconstruction and system level investigation of the

844 metabolic network of Methylobacterium extorquens AM1. BMC Systems
845 Biology 5:189.

846 8. Fu Y, He L, Reeve J, Beck DAC, Lidstrom ME. 2019. Core Metabolism
847 Shifts during Growth on Methanol versus Methane in the Methanotroph
848 Methylomicrobium buryatense 5GB1. MBio 10.

849 9. Niedenführ S, Wiechert W, Nöh K. 2015. How to measure metabolic
850 fluxes: a taxonomic guide for 13C fluxomics. Current Opinion in
851 Biotechnology 34:82–90.

852 10. Heux S, Bergès C, Millard P, Portais J-C, Létisse F. 2017. Recent advances
853 in high-throughput 13 C-fluxomics. Current Opinion in Biotechnology
854 43:104–109.

855 11. Schendel FJ, Bremmon CE, Flickinger MC, Guettler M, Hanson RS. 1990.
856 L-lysine production at 50 degrees C by mutants of a newly isolated and
857 characterized methylotrophic Bacillus sp. Appl Environ Microbiol 56:963–
858 970.

859 12. Pfeifenschneider J, Brautaset T, Wendisch VF. 2017. Methanol as carbon
860 substrate in the bio-economy: Metabolic engineering of aerobic
861 methylotrophic bacteria for production of value-added chemicals:
862 Methanol as carbon substrate in the bio-economy. Biofuels, Bioproducts
863 and Biorefining 11:719–731.

864 13. Iaquaniello G, Centi G, Salladini A, Palo E, Perathoner S. 2018. Waste to
865 Chemicals for a Circular Economy. Chemistry 24:11831–11839.

866 14. Müller JEN, Heggeset TMB, Wendisch VF, Vorholt JA, Brautaset T. 2015.
867 Methylotrophy in the thermophilic Bacillus methanolicus, basic insights
868 and application for commodity production from methanol. Applied
869 Microbiology and Biotechnology 99:535–551.

15. Komives CF, Cheung LY-Y, Pluschkell SB, Flickinger MC. 2005. Growth of Bacillus methanolicus in seawater-based media. J Ind Microbiol Biotechnol 32:61–66.

16. Naerdal I, Pfeifenschneider J, Brautaset T, Wendisch VF. 2015. Methanol-based cadaverine production by genetically engineered *B acillus methanolicus* strains: Cadaverine production by Bacillus methanolicus. Microbial Biotechnology 8:342–350.

17. Irla M, Nærdal I, Brautaset T, Wendisch VF. 2017. Methanol-based γ-aminobutyric acid (GABA) production by genetically engineered Bacillus methanolicus strains. Industrial Crops and Products 106:12–20.

18. Drejer EB, Hakvåg S, Irla M, Brautaset T. 2018. Genetic Tools and Techniques for Recombinant Expression in Thermophilic Bacillaceae. Microorganisms 6.

19. Irla M, Heggeset TMB, Nærdal I, Paul L, Haugen T, Le SB, Brautaset T, Wendisch VF. 2016. Genome-Based Genetic Tool Development for Bacillus methanolicus: Theta- and Rolling Circle-Replicating Plasmids for Inducible Gene Expression and Application to Methanol-Based Cadaverine Production. Frontiers in Microbiology 07.

20. Schultenkämper K, Brito LF, López MG, Brautaset T, Wendisch VF. 2019. Establishment and application of CRISPR interference to affect sporulation, hydrogen peroxide detoxification, and mannitol catabolism in the methylotrophic thermophile Bacillus methanolicus. Appl Microbiol Biotechnol 103:5879–5889.

21. Heggeset TMB, Krog A, Balzer S, Wentzel A, Ellingsen TE, Brautaset T. 2012. Genome Sequence of Thermotolerant Bacillus methanolicus: Features and Regulation Related to Methylotrophy and Production of l-

Lysine and l-Glutamate from Methanol. Appl Environ Microbiol 78:5170–5181.

22. López MG, Irla M, Brito LF, Wendisch VF. 2019. Characterization of D-Arabitol as Newly Discovered Carbon Source of Bacillus methanolicus. Front Microbiol 10:1725.

23. Povelainen M, Eneyskaya EV, Kulminskaya AA, Ivanen DR, Kalkkinen N, Neustroev KN, Miasnikov AN. 2003. Biochemical and genetic characterization of a novel enzyme of pentitol metabolism: D-arabitol-phosphate dehydrogenase. Biochem J 371:191–197.

24. Irla M, Neshat A, Winkler A, Albersmeier A, Heggeset TMB, Brautaset T, Kalinowski J, Wendisch VF, Rückert C. 2014. Complete genome sequence of Bacillus methanolicus MGA3, a thermotolerant amino acid producing methylotroph. J Biotechnol 188:110–111.

25. Irla M, Neshat A, Brautaset T, Rückert C, Kalinowski J, Wendisch VF. 2015. Transcriptome analysis of thermophilic methylotrophic Bacillus methanolicus MGA3 using RNA-sequencing provides detailed insights into its previously uncharted transcriptional landscape. BMC Genomics 16:73.

26. Müller JEN, Litsanov B, Bortfeld-Miller M, Trachsel C, Grossmann J, Brautaset T, Vorholt JA. 2014. Proteomic analysis of the thermophilic methylotroph Bacillus methanolicus MGA3. Proteomics 14:725–737.

27. Müller JEN, Meyer F, Litsanov B, Kiefer P, Vorholt JA. 2015. Core pathways operating during methylotrophy of Bacillus methanolicus MGA3 and induction of a bacillithiol-dependent detoxification pathway upon formaldehyde stress. Mol Microbiol 98:1089–1100.

921 28. Carnicer M, Vieira G, Brautaset T, Portais J-C, Heux S. 2016. Quantitative
922 metabolomics of the thermophilic methylotroph Bacillus methanolicus.
923 Microbial Cell Factories 15.
924 29. Izhaki I, Fridman S, Gerchman Y, Halpern M. 2013. Variability of bacterial
925 community composition on leaves between and within plant species.
926 Curr Microbiol 66:227–235.
927 30. Fall R, Benson AA. 1996. Leaf methanol — the simplest natural product
928 from plants. Trends in Plant Science 1:296–301.
929 31. Mashego MR, Wu L, Van Dam JC, Ras C, Vinke JL, Van Winden WA, Van
930 Gulik WM, Heijnen JJ. 2004. MIRACLE: mass isotopomer ratio analysis of
931 U-13C-labeled extracts. A new method for accurate quantification of
932 changes in concentrations of intracellular metabolites. Biotechnol Bioeng
933 85:620–628.
934 32. Kiefer P, Nicolas C, Letisse F, Portais J-C. 2007. Determination of carbon
935 labeling distribution of intracellular metabolites from single fragment
936 ions by ion chromatography tandem mass spectrometry. Anal Biochem
937 360:182–188.
938 33. Millard P, Delépine B, Guionnet M, Heuillet M, Bellvert F, Létisse F. IsoCor:
939 isotope correction for high-resolution MS labeling experiments.
940 Bioinformatics.
941 34. van der Heijden RT, Romein B, Heijnen JJ, Hellinga C, Luyben KC. 1994.
942 Linear constrain relations in biochemical reaction systems III. Sequential
943 application of data reconciliation for sensitive detection of systematic
944 errors. Biotechnol Bioeng 44:781–791.
945 35. Dauner M, Sauer U. 2001. Stoichiometric growth model for riboflavin-
946 producing Bacillus subtilis. Biotechnol Bioeng 76:132–143.

947 36. Dauner M, Bailey JE, Sauer U. 2001. Metabolic flux analysis with a
948 comprehensive isotopomer model in Bacillus subtilis. Biotechnol Bioeng
949 76:144–156.
950 37. Stephanopoulos G, Locher G, Duff MJ, Kamimura R, Stephanopoulos G.
951 1997. Fermentation database mining by pattern recognition. Biotechnol
952 Bioeng 53:443–452.
953 38. Boudah S, Olivier M-F, Aros-Calt S, Oliveira L, Fenaille F, Tabet J-C, Junot
954 C. 2014. Annotation of the human serum metabolome by coupling three
955 liquid chromatography methods to high-resolution mass spectrometry. J
956 Chromatogr B Analyt Technol Biomed Life Sci 966:34–47.
957 39. Massou S, Nicolas C, Letisse F, Portais J-C. 2007. NMR-based fluxomics:
958 quantitative 2D NMR methods for isotopomers analysis. Phytochemistry
959 68:2330–2340.
960 40. Massou S, Nicolas C, Letisse F, Portais J-C. 2007. Application of 2D-TOCSY
961 NMR to the measurement of specific(13C-enrichments in complex
962 mixtures of 13C-labeled metabolites. Metab Eng 9:252–257.
963 41. Sokol S, Millard P, Portais J-C. 2012. influx_s: increasing numerical
964 stability and precision for metabolic flux analysis in isotope labelling
965 experiments. Bioinformatics 28:687–693.
966 42. Sauer U, Hatzimanikatis V, Hohmann HP, Manneberg M, van Loon AP,
967 Bailey JE. 1996. Physiology and metabolic fluxes of wild-type and
968 riboflavin-producing Bacillus subtilis. Appl Environ Microbiol 62:3687–
969 3696.
970 43. Hanahan D. 1983. Studies on transformation of Escherichia coli with
971 plasmids. J Mol Biol 166:557–580.

44. Studier FW, Moffatt BA. 1986. Use of bacteriophage T7 RNA polymerase to direct selective high-level expression of cloned genes. J Mol Biol 189:113–130.

45. Green MR, Sambrook J, Sambrook J. 2012. Molecular cloning: a laboratory manual4th ed. Cold Spring Harbor Laboratory Press, Cold Spring Harbor, N.Y.

46. Eikmanns BJ, Thum-Schmitz N, Eggeling L, Lüdtke KU, Sahm H. 1994. Nucleotide sequence, expression and transcriptional analysis of the Corynebacterium glutamicum gltA gene encoding citrate synthase. Microbiology (Reading, Engl) 140 (Pt 8):1817–1828.

47. Gibson DG, Young L, Chuang R-Y, Venter JC, Hutchison CA, Smith HO. 2009. Enzymatic assembly of DNA molecules up to several hundred kilobases. Nat Methods 6:343–345.

48. Mandel M, Higa A. 1970. Calcium-dependent bacteriophage DNA infection. J Mol Biol 53:159–162.

49. Lindner SN, Vidaurre D, Willbold S, Schoberth SM, Wendisch VF. 2007. NCgl2620 encodes a class II polyphosphate kinase in Corynebacterium glutamicum. Appl Environ Microbiol 73:5026–5033.

50. Laemmli UK. 1970. Cleavage of structural proteins during the assembly of the head of bacteriophage T4. Nature 227:680–685.

51. Bradford MM. 1976. A rapid and sensitive method for the quantitation of microgram quantities of protein utilizing the principle of protein-dye binding. Analytical Biochemistry 72:248–254.

52. Stolzenberger J, Lindner SN, Persicke M, Brautaset T, Wendisch VF. 2013. Characterization of fructose 1,6-bisphosphatase and sedoheptulose 1,7-bisphosphatase from the facultative ribulose monophosphate cycle methylotroph Bacillus methanolicus. J Bacteriol 195:5112–5122.

53. Nordling E, Jörnvall H, Persson B. 2002. Medium-chain dehydrogenases/reductases (MDR). Family characterizations including genome comparisons and active site modeling. Eur J Biochem 269:4267–4276.

54. Persson B, Hedlund J, Jörnvall H. 2008. Medium- and short-chain dehydrogenase/reductase gene and protein families : the MDR superfamily. Cell Mol Life Sci 65:3879–3894.

55. Soroka NV, Kulminskaya AA, Eneyskaya EV, Shabalin KA, Uffimtcev AV, Povelainen M, Miasnikov AN, Neustroev KN. 2005. Synthesis of arabinitol 1-phosphate and its use for characterization of arabinitol-phosphate dehydrogenase. Carbohydr Res 340:539–546.

56. Millard P, Sokol S, Letisse F, Portais J-C. 2014. IsoDesign: a software for optimizing the design of 13C-metabolic flux analysis experiments. Biotechnol Bioeng 111:202–208.

57. Wiechert W, Nöh K. 2005. From Stationary to Instationary Metabolic Flux Analysis, p. 145–172. *In* Kragl, U (ed.), Technology Transfer in Biotechnology. Springer Berlin Heidelberg, Berlin, Heidelberg.

58. Nöh K, Grönke K, Luo B, Takors R, Oldiges M, Wiechert W. 2007. Metabolic flux analysis at ultra short time scale: isotopically non-stationary 13C labeling experiments. J Biotechnol 129:249–267.

59. Brautaset T, Williams MD, Dillingham RD, Kaufmann C, Bennaars A, Crabbe E, Flickinger MC. 2003. Role of the Bacillus methanolicus citrate synthase II gene, citY, in regulating the secretion of glutamate in L-lysine-secreting mutants. Appl Environ Microbiol 69:3986–3995.

60. Shiio I, Sano K, Nakamori S. December 1972. Method of producing l-lysine by fermentation. US3707441A.

1025 61. Szenk M, Dill KA, de Graff AMR. 2017. Why Do Fast-Growing Bacteria
1026 Enter Overflow Metabolism? Testing the Membrane Real Estate
1027 Hypothesis. Cell Syst 5:95–104.
1028 62. Bernal V, Castaño-Cerezo S, Cánovas M. 2016. Acetate metabolism
1029 regulation in Escherichia coli: carbon overflow, pathogenicity, and
1030 beyond. Appl Microbiol Biotechnol 100:8985–9001.
1031 63. Enjalbert B, Millard P, Dinclaux M, Portais J-C, Létisse F. 2017. Acetate
1032 fluxes in Escherichia coli are determined by the thermodynamic control
1033 of the Pta-AckA pathway. Sci Rep 7:42135.
1034 64. Polen T, Rittmann D, Wendisch VF, Sahm H. 2003. DNA microarray
1035 analyses of the long-term adaptive response of Escherichia coli to
1036 acetate and propionate. Appl Environ Microbiol 69:1759–1774.
1037 65. Jakobsen ØM, Benichou A, Flickinger MC, Valla S, Ellingsen TE, Brautaset
1038 T. 2006. Upregulated transcription of plasmid and chromosomal ribulose
1039 monophosphate pathway genes is critical for methanol assimilation rate
1040 and methanol tolerance in the methylotrophic bacterium Bacillus
1041 methanolicus. J Bacteriol 188:3063–3072.
1042 66. Anthony C. 1991. Assimilation of carbon by methylotrophs.
1043 Biotechnology 18:79–109.
1044 67. Stolzenberger J, Lindner SN, Wendisch VF. 2013. The methylotrophic
1045 Bacillus methanolicus MGA3 possesses two distinct fructose 1,6-
1046 bisphosphate aldolases. Microbiology (Reading, Engl) 159:1770–1781.
1047 68. Chistoserdova LV, Chistoserdov AY, Schklyar NL, Baev MV, Tsygankov YD.
1048 1991. Oxidative and assimilative enzyme activities in continuous
1049 cultures of the obligate methylotroph Methylobacillus flagellatum.
1050 Antonie Van Leeuwenhoek 60:101–107.

69. Bennett RK, Gonzalez JE, Whitaker WB, Antoniewicz MR, Papoutsakis ET. 2018. Expression of heterologous non-oxidative pentose phosphate pathway from Bacillus methanolicus and phosphoglucose isomerase deletion improves methanol assimilation and metabolite production by a synthetic Escherichia coli methylotroph. Metabolic Engineering 45:75–85.

70. Bozdag A, Komives C, Flickinger MC. 2015. Growth of Bacillus methanolicus in 2 M methanol at 50 °C: the effect of high methanol concentration on gene regulation of enzymes involved in formaldehyde detoxification by the ribulose monophosphate pathway. J Ind Microbiol Biotechnol 42:1027–1038.

71. Chistoserdova L, Kalyuzhnaya MG, Lidstrom ME. 2009. The expanding world of methylotrophic metabolism. Annu Rev Microbiol 63:477–499.

72. Oh Y-K, Palsson BO, Park SM, Schilling CH, Mahadevan R. 2007. Genome-scale reconstruction of metabolic network in Bacillus subtilis based on high-throughput phenotyping and gene essentiality data. J Biol Chem 282:28791–28799.

73. Gonzalez JE, Long CP, Antoniewicz MR. 2017. Comprehensive analysis of glucose and xylose metabolism in Escherichia coli under aerobic and anaerobic conditions by 13C metabolic flux analysis. Metab Eng 39:9–18.

74. Revelles O, Millard P, Nougayrède J-P, Dobrindt U, Oswald E, Létisse F, Portais J-C. 2013. The carbon storage regulator (Csr) system exerts a nutrient-specific control over central metabolism in Escherichia coli strain Nissle 1917. PLoS ONE 8:e66386.

75. Spaans SK, Weusthuis RA, van der Oost J, Kengen SWM. 2015. NADPH-generating systems in bacteria and archaea. Front Microbiol 6:742.

76. Arfman N, Hektor HJ, Bystrykh LV, Govorukhina NI, Dijkhuizen L, Frank J. 1997. Properties of an NAD(H)-containing methanol dehydrogenase and

its activator protein from Bacillus methanolicus. Eur J Biochem 244:426–433.

Figure descriptions

Fig. 1: Flux map of *B. methanolicus* central metabolism relative to substrate intake for methanol (A), mannitol (B) and arabitol (C). The thickness of the reaction lines represent the flux proportions relative to substrate incorporation into the metabolism: hps (A), Manupt (B), Araupt (C). Flux proportions were averaged among the biological replicates ($n_{methanol}$=2, $n_{arabitol}$ = $n_{mannitol}$ = 3). The direction of the reaction arrows represent the estimated net flux directionality. Large grey arrows represent a flux directed toward amino acid synthesis and biomass requirements for growth. Pathways discussed in the text are represented by a background patch of color. Metabolites are represented by circles and have a solid bottom half if they are duplicated on the same panel, as per recommended by the SBGN standard. Metabolites subjected to experimental measurement of ^{13}C labelling are marked by a yellow box. Some intermediate metabolites are not needed for ^{13}C-MFA and are consequently lumped in mannitol and arabitol models (B, C); the same metabolites can be explicitly modelled in methanol model (A) since non-stationary ^{13}C-MFA requires all intermediates pools (e.g.: G3P, Cit, Aco). Reactions toward amino acid pools and biomass are not represented.

Fig. 2: Alternative assimilation pathways of D-arabitol with an example of the measured and expected labeling of Rib5P. Arabitol

entry point into the metabolism is expected to be Ribu5P or Xyl5P, depending on the substrate specificity of the PTS system and the arabitol phosphate dehydrogenase. Taking [5-^{13}C]arabitol as an example, we show that the labeling of downstream metabolites can be used to identify which pathway is operating *in vivo* (Ribu5P, orange; Xyl5P, blue). We exemplify our approach with one data point: the NMR specific enrichment of Rib5P and the associated estimates from the best fit of different scenarios in which PTS1 or PTS5 are allowed to carry flux in the model (barplot). Unlike the others, the model in which only PTS5 was allowed to carry flux did not fit the data (red crossmark, ✘). Circles are carbon atoms: solid for ^{13}C (●), empty for ^{12}C (○), dotted when irrelevant.

Fig. 3: Estimated absolute fluxes (mmol/gDCW/h) for methanol (blue), mannitol (orange) and arabitol (green). The bars represent the average of the estimated absolute net flux for each biological replicate (black dot), and the error bar is the associated standard deviation ($n_{methanol}$ = 2, $n_{arabitol}$ = $n_{mannitol}$ = 3).

Fig. 4: Estimated absolute rates of production and consumption of NADPH, NADH/FADH2, and ATP. Rates (mmol/gDCW/h) are calculated as the sum of the estimated flux of the reactions modeled in the MFA that are expected to produce (positive value) or consume (negative value) those cofactors. Values are averaged over the biological replicates and the error bars are the associated standard deviation ($n_{methanol}$ = 2, $n_{arabitol}$ = $n_{mannitol}$ = 3). The growth requirements (“biomass”, red) are computed from measures on *B. subtilis* (mmol/gDCW) and the growth rates we observed. Production and

consumption rates should be balanced in our conditions, so we mark putative production/consumption rates as “unknown” to complete the balance when needed. The full production of NADH and FADH2 is assumed to be consumed in the respiratory chain (“oxidative phosphorylation”) and to produce ATP (with $P/O_{NADH} = 1.5$, $P/O_{FADH2} = 1$). We modeled the PTS systems of mannitol and arabitol as consumers of one equivalent ATP (in “uptake”). NADPH production: glucose 6-phosphate dehydrogenase (*zwf*), phosphogluconate dehydrogenase (*gnd*), isocitrate dehydrogenase (*idh*), and methylenetetrahydrofolate dehydrogenase from the linear detoxification pathway (detox). NADH production: glyceraldehyde-3-phosphate dehydrogenase (*pgk*), pyruvate dehydrogenase (*pdh*), 2-oxoglutarate dehydrogenase (*akgdh*), malate dehydrogenase (assimilated to *fum*), methanol, mannitol and arabitol dehydrogenase (*mdh*, manupt, araupt), and formate dehydrogenase from the linear detoxification pathway (detox). FADH2 production: succinate dehydrogenase (*fum*). ATP consumption: 6-phosphofructokinase (*pfk*), PTS systems of mannitol and arabitol (manupt, araupt). ATP production: phosphoglycerate kinase (*pgk*), pyruvate kinase (*pyk*), succinyl-CoA synthetase (assimilated to *akgdh*), acetate kinase (*out_Ac*), and formate-tetrahydrofolate ligase from the linear detoxification pathway (detox).

Tables

Table 1. Strains, primers and plasmids used in this study.

Strain, plasmid or primer	Relevant characteristics	Reference
Strains		
E. coli DH5α	F^- *thi*-1 *endA1 hsdR17*(r^- m^-) *supE44* Δ*lacU169* (φ80*lacZ*ΔM15) *recA1 gyrA96 relA1*	(43)
E. coli BL21 (DE3)	F^- *ompT hsdSB*(r_B^- m_B^-) *gal dcm* (DE3)	(44)
B. methanolicus MGA3	Wild type strain (ATCC 53907)	(11)
Plasmids		
pET16b	Amp^R; overproduction of decahistidine-tagged proteins in *E. coli* (pBR322 oriVE.c., *PT7*, *lacI*)	Novagen
pET16b-*atlD*	pET16b derivative for the production of *B. methanolicus* His_{10}-tagged AtlD from *E. coli* BL21 (DE3)	This study

pET16b-*atlF*	pET16b derivative for the production of *B. methanolicus* His_{10}-tagged AtlF from *E. coli* BL21 (DE3)	This study

Primers	**Sequence [5’ → 3’]**	**Characteristics**
P192	agcttcctttcgggctttgttagcagcc gTTAATCAATAGGTGTCAACAAT AC	Amplification of *atlD* for pET16b-*atlD*
P193	gccatatcgaaggtcgtcatatgctcg agATGAAAGCTTTAGTCAAAAA AG	
P194	agcttcctttcgggctttgttagcagcc gTTATGATTTTTCTGGATGGAAG	Amplification of *atlF* for pET16b-*atlF*
P195	gccatatcgaaggtcgtcatatgctcg agATGAAAGCATTAAAGCTGTA TG	

1147 Amp^R: ampicillin resistance; overlapping regions are shown in lower case.

Table 2. Kinetic data of purified AtlD and AtlF

Condition[a]: protein, substrate, cofactor[b]	**Substrate K_M (mM)**	**V_{max} (U mg^{-1})[c]**	**V_{max} / K_M**
AtlD, Xyl5P, NADH	0.07 ± 0.03	1.33 ± 0.23	19
AtlD, Ribu5P, NADH	1.21 ± 0.42	0.49 ± 0.06	0.4
AtlF, Xyl5P, NADH	0.18 ± 0.05	0.11 ± 0.01	0.6

[a] The following reactions were also analysed, but no significant activity (i.e. < 0.05 U mg^{-1}) could be detected: AtlD, Ribu5P, NADPH; AtlF, Xyl5P, NADPH; AtlF, Ribu5P, NADH; AtlF, Ribu5P, NADPH.

[b] Cofactor K_M values were analysed using 0.2 mM Xyl5P and were 0.01 ± 0.01 and 0.11 ± 0.09 for NADH and NADPH, respectively.

[c] The V_{max} for AtlD, Xyl5P, NADPH was calculated using 0.2 mM of substrate and 0.3 mM of cofactor, and resulted in 0.24 ± 0.06 U mg^{-1}.

Table 3: Physiological parameters of *B. methanolicus* cultures used for Metabolic Flux Analysis. Growth rate and biomass quantities were deduced from OD_{600} measurements in the exponential growth phase. Carbon source evolution rates were measured from supernatant samples and analyzed by NMR. Labelled CO_2 was monitored by MS in the bioreactor's outgoing gas flow. All cultures were aerobic. n.a.: not measured; n.d.: not detected. The uncertainties shown are standard errors between biological replicates.

	Methanol (CH3OH)	**Mannitol** (C6H14O6)	**Arabitol** (C5H12O5)	
Method	13C INST-MFA bioreactor (n=2)	[1-13C] MFA flask (n=3)	Mix. [1-13C] & [2-13C] MFA, flask (n=3)	[5-13C] MFA flask (n=3)
Growth rate [h-1]	0.46 ± 0.002	0.36 ± 0.02	0.15 ± 0.004	0.1411 ± 0.02
Biomass yield [gDCW/gSubstrate]	0.55 ± 0.01	0.34 ± 0.08	0.19 ± 0.02	0.23 ± 0.02
C source [mmolC/gDCW/h]	21.9 ± 2.2	36 ± 7.3	21.4 ± 1.2	24.5 ± 0.75
$CO2_{out}$ [mmol/gDCW/h]	7.6 ± 0.04	n.a.	n.a.	n.a.
$Acetate_{out}$ [mmol/gDCW/h]	n.d.	1.75 ± 0.32	n.d.	n.d.

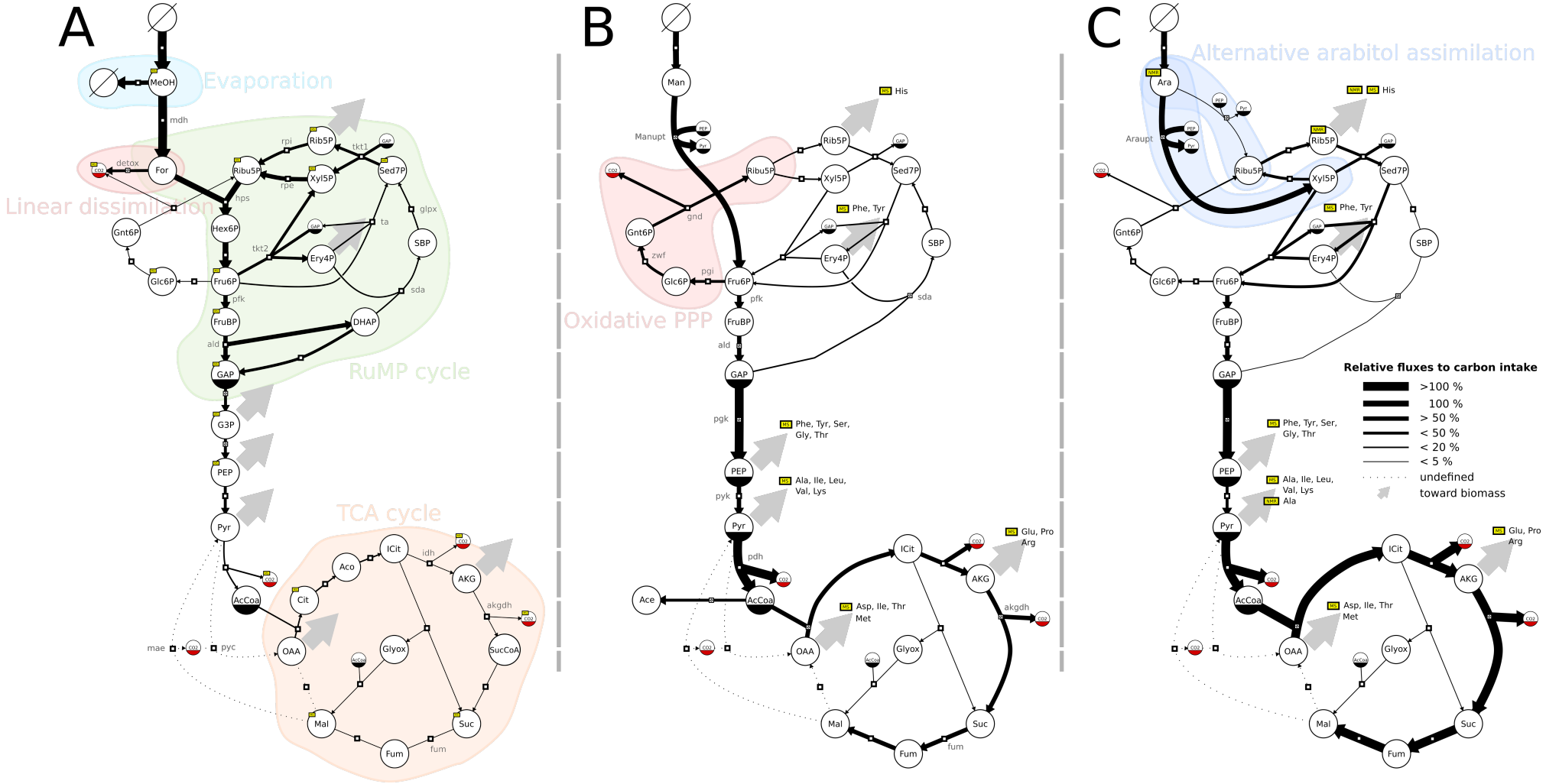

Fig. 1: Flux map of *B. methanolicus* central metabolism relative to substrate intake for methanol (A), mannitol (B) and arabitol (C). The thickness of the reaction lines represent the flux proportions relative to substrate incorporation into the metabolism: hps (A), Manupt (B), Araupt (C). Flux proportions were averaged among the biological replicates ($n_{methanol}$=2, $n_{arabitol}$ = $n_{mannitol}$ = 3). The direction of the reaction arrows represent the estimated net flux directionality. Large grey arrows represent a flux directed toward amino acid synthesis and biomass requirements for growth. Pathways discussed in the text are represented by a background patch of color. Metabolites are represented by circles and have a solid bottom half if they are duplicated on the same panel, as per recommended by the SBGN standard. Metabolites subjected to experimental measurement of ^{13}C labeling are marked by a yellow box. Some intermediate metabolites are not needed for ^{13}C-MFA and are consequently lumped in mannitol and arabitol models (B, C); the same metabolites can be explicitly modeled in methanol model (A) since non-stationary ^{13}C-MFA requires all intermediates pools (e.g.: G3P, Cit, Aco). Reactions toward amino acid pools and biomass are not represented.

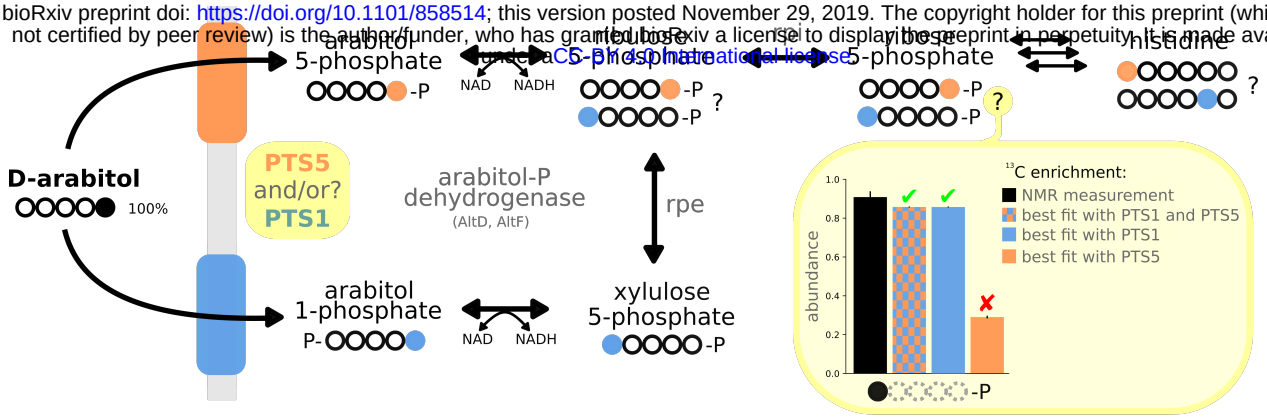

Fig. 2: Alternative assimilation pathways of D-arabitol with an example of the measured and expected labeling of Rib5P. Arabitol entry point into the metabolism is expected to be Ribu5P or Xyl5P, depending on the substrate specificity of the PTS system and the arabitol phosphate dehydrogenase. Taking [5-13C]arabitol as an example, we show that the labeling of downstream metabolites can be used to identify which pathway is operating *in vivo* (Ribu5P, orange; Xyl5P, blue). We exemplify our approach with one data point: the NMR specific enrichment of Rib5P and the associated estimates from the best fit of different scenario in which PTS1 or PTS5 are allowed to carry flux in the model (barplot). Unlike the others, the model in which only PTS5 was allowed to carry flux did not fit the data (red cross-mark, ✘). Circles are carbon atoms: solid for ^{13}C (●), empty for ^{12}C (○), dotted when irrelevant.

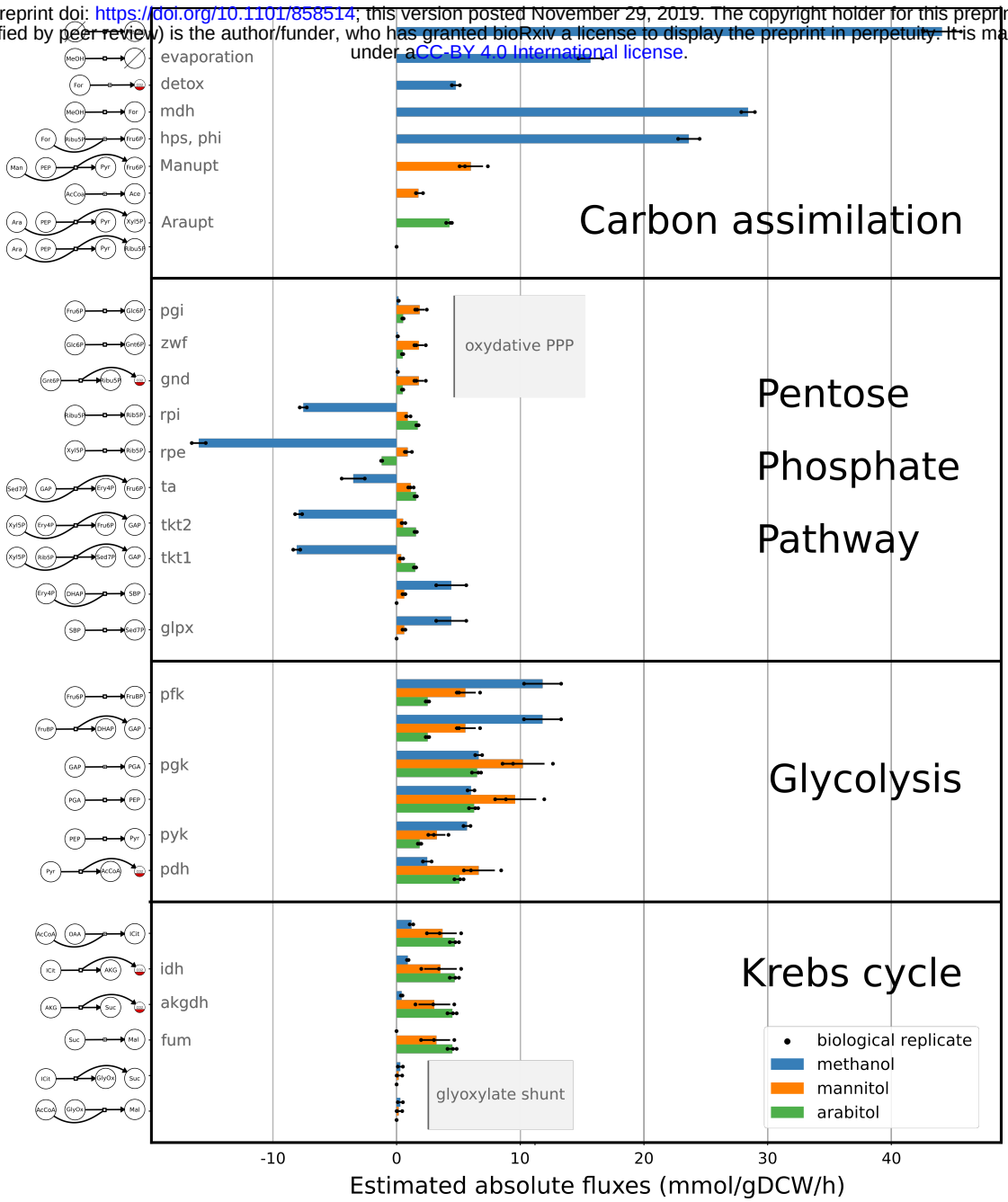

Fig. 3: Estimated absolute fluxes (mmol/gDCW/h) for methanol (blue), mannitol (orange) and arabitol (green). The bars represent the average of the estimated absolute net flux for each biological replicate (black dot), and the error bar is the associated standard deviation ($n_{methanol}$=2, $n_{arabitol}$ = $n_{mannitol}$ = 3).

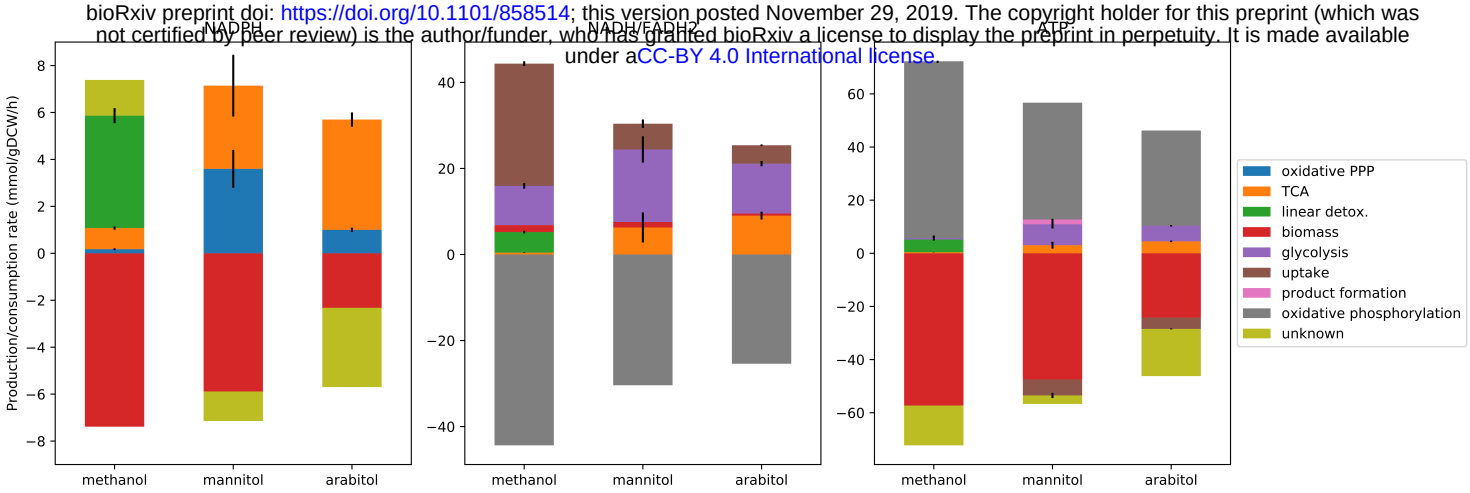

Fig. 4: Estimated absolute rates of production and consumption of NADPH, NADH/FADH2, and ATP. Rates (mmol/gDCW/h) are calculated as the sum of the estimated flux of the reactions modeled in the MFA that are expected to produce (positive value) or consume (negative value) those cofactors. Values are averaged over the biological replicates and the error bars are the associated standard deviation ($n_{methanol}$=2, $n_{arabitol}$ = $n_{mannitol}$ = 3). The growth requirements ("biomass", red) are computed from measures on *B. subtilis* (mmol/gDCW) and the growth rates we observed. Production and consumption rates should be balanced in our conditions, so we mark putative production/consumption rates as "unknown" to complete the balance when needed. The full production of NADH and FADH2 is assumed to be consumed in the respiratory chain ("oxidative phophorylation") and to produce ATP (with P/O_{NADH}=1.5, P/O_{FADH2}=1). We modeled the PTS systems of mannitol and arabitol as consumers of one equivalent ATP (in "uptake"). NADPH production: glucose-6-phosphate dehydrogenase (*zwf*), phosphogluconate dehydrogenase (*gnd*), isocitrate dehydrogenase (*idh*), and methylenetetrahydrofolate dehydrogenase from the linear detoxification pathway (detox). NADH production: glyceraldehyde-3-phosphate dehydrogenase (*pgk*), pyruvate dehydrogenase (*pdh*), 2-oxoglutarate dehydrogenase (*akgdh*), malate dehydrogenase (assimilated to *fum*), methanol mannitol and arabitol dehydrogenase (*mdh*, manupt, araupt), and formate dehydrogenase from the linear detoxification pathway (detox). FADH2 production: succinate dehydrogenase (*fum*). ATP consumption: 6-phosphofructokinase (*pfk*), PTS systems of mannitol and arabitol (manupt, araupt). ATP production: phosphoglycerate kinase (*pgk*), pyruvate kinase (*pyk*), succinyl-CoA synthetase (assimilated to *akgdh*), acetate kinase (*out_Ac*), and formate-tetrahydrofolate ligase from the linear detoxification pathway (detox).